Supervisors:

- Joshi, S.
- Della Santina, C.

Date of defense: 12th of September 2023
Awarding Institute: The Delft University of Technology

Towards the Development of a Passive Adaptive Variable Stiffness Exosuit

Tim Verburg

***Abstract*—A substantial portion of workplace-related injuries stem from sprains, strains, and muscle tears, with a significant proportion occurring in the upper body, particularly the shoulder. To address these issues, there is a growing interest in utilizing supportive devices like exoskeletons that often face challenges such as bulkiness, high costs, and parasitic forces, which have hindered their widespread adoption. Exosuits, an alternative to exoskeletons, offer potential solutions by primarily employing fabrics and leveraging the human body to transmit forces, eliminating the need for cumbersome and expensive external frames. A user study involving a passive-adaptive exosuit equipped with a controllable pretension spring showed a reduction in muscle effort while being limited to controlling only the system's equilibrium position. It was theorized that the addition of a variable stiffness mechanism with controllable pretension and stiffness could eliminate observed issues and further increase muscle effort reduction, forming the need for a variable stiffness mechanism. The vast majority of existing variable stiffness solutions are developed for use in joints as opposed to being designed for a linear motion and are thus not ideal for application in an exosuit. Additionally, the fusion of variable stiffness mechanisms and exosuits has not been studied extensively, with no studies using a variable stiffness mechanism capable of controlling both the stiffness and equilibrium position in an exosuit. This work presents the results of the user study, the development and testing of a variable linear stiffness mechanism for a linear motion capable of controlling the stiffness and equilibrium position, and the integration of said actuator in an exosuit.**

I. Introduction

In 2020, the majority of workplace-related injuries in the United States were due to sprains, strains, and tears of muscles, of which 31% was in the upper extremities, primarily the shoulder [1]. These injuries affected over 255,000 people with a median time away from work being 14 days. Suits, both rigid and flexible, that could support or enhance the wearer could provide a solution to this problem and have been shown to reduce injuries using passive exoskeletons [2]. Such supportive devices can be categorized into one of two types, an exoskeleton, or an exosuit [3], with the distinction being the presence of a compressive load-bearing frame. Exoskeletons are generally heavier, more expensive, and struggle with parasitic forces in the joints due to misalignments. Exosuits, on the other hand, use the existing joints in combination with fabrics to create a lightweight supportive device that can be more comfortable than an exoskeleton while still assisting the wearer. These suits have not seen major adoption, thought to be primarily due to the limited operation duration or ease of use. Most existing suits are either completely passive, like the first suit in figure 1 and thus limiting adjustability, or have rigid actuators that do not inherently allow for compliance [3].

The code and CAD files for this thesis can be found at https://github.com/Tverburg1/ExoTendonStiffnessControl

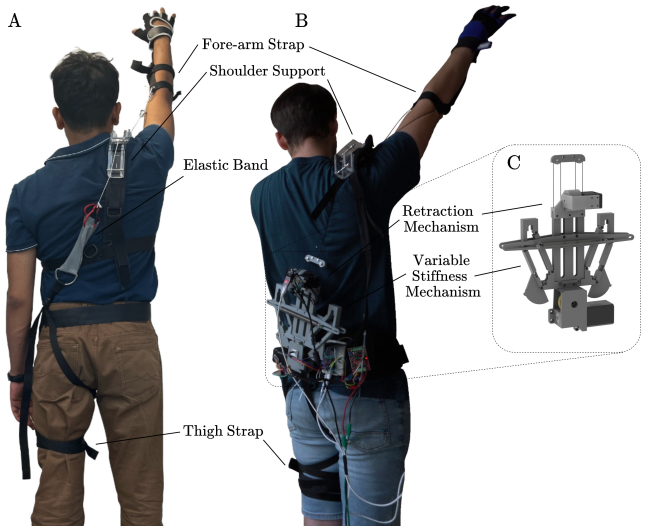

Fig. 1: (A) The original entirely passive exosuit utilizing an elastic band [4]. (B) The final integrated exosuit with the variable stiffness mechanism. (C) The final version of the variable stiffness mechanism.

Human-machine interaction has classically been rigid, with later advances using torque control to create control-based compliance [5]. However, this comes at the cost of energy expenditure, which is crucial for mobile solutions. Control-based compliance, such as impedance control, has an inherent delay that could make the interaction unstable or unsafe as unwanted effects might have already occurred before the control-based solution has time to react to the event [6], [7]. Mechanical variable stiffness solutions have been designed such that they only require energy when changing the stiffness parameters or the output of the system. Some of these systems only have one degree of freedom, generally used to adjust the pretension of a spring, leading to a different perceived stiffness for a given displacement [8]–[14]. Other systems utilize antagonistic nonlinear springs, either premade or created from linear springs using a variety of mechanisms [15]–[17]. These can then be combined with pretensioning mechanisms in order to control both the perceived stiffness and equilibrium position of the system. The last major group of variable stiffness actuators is that of structure-based variable stiffness, which obtains variable stiffness by changing the structural properties

of the system such as the transmission ratio or the effective length of a spring [18]–[23]. All of these variable stiffness solutions are designed to be used in a joint as opposed to being used for a linear motion.

Some supportive devices exist that have implemented such variable stiffness mechanisms to be compliant, which primarily consists of exoskeletons [24]–[26], although similar designs exist also for exosuits [27], [28]. Notable is that most of these variable stiffness solutions only have one degree of freedom that is dedicated to pretensioning a spring and thus cannot simultaneously control both the equilibrium position and perceived stiffness.

The need for a variable stiffness actuator stems from the user study that constitutes the first contribution of this MSc thesis, which I will discuss in section II. This study was performed using an exosuit that was the result of the continued development of the suit seen in figure 1 that was used in [4]. The exosuit in the user study was designed to assist the right shoulder flexion and had the ability to pretension a spring to change the equilibrium position and thus the assistive force for a given elevation of the arm. However, with only the ability to adjust the pretension, it was observed that the range of assistance of the suit was limited, as in the event a large force had to be applied the spring needed to be pre-tensioned significantly, possibly forcing the wearer into uncomfortable configurations. A variable stiffness mechanism would be able to achieve the same desired force by instead increasing the stiffness with a lower required pretension, with the possibility of completely bearing the load of the arm by setting the mechanism to an infinite stiffness.

To summarize, the goal of this work is to briefly present the results from the user study that formed the need to create a variable stiffness solution for a linear motion to be applied in the previously mentioned exosuit with the purpose of filling the two academic gaps, (i) a linear motion variable stiffness mechanism with a linear stiffness output capable of both equilibrium and stiffness control, and (ii) using a variable stiffness mechanism with equilibrium and stiffness control in an exosuit. This work focuses primarily on the first part and will present the designed solution integrated into an exosuit as a proof of concept.

First, the results from the user study, illustrating the need for the variable stiffness actuator, are presented in section II. Then, the design parameters based on this user study will be defined in section III, after which the design and working principle will be explained in section IV. This design is then subject to a series of experiments, presented in section V, to validate the functionality of the mechanism and highlight areas of improvement. Finally, section VII will draw the final conclusions and discuss the future possibilities and improvements.

II. Supporting User Study

To study the efficacy of the passive-adaptive exosuit, used in the user study mentioned in the introduction which is based on the previous suit from [4], as seen in figure 1, augmented with a motor to pretension a spring on the upper arm. Passive-adaptive refers to the actuation strategy used which is to only power the motor when changing the pretension of the spring, resembling the active part, with the suit otherwise functioning as a passive exosuit. The suit is equipped with an inertial measurement unit that allows for the measuring of the angle and velocity of the arm which is used in a mapping that is the result of a precomputed biomechanically aware optimization using OpenSim, a musculoskeletal simulation program, to minimize the cumulative muscle effort for a given motion by computing the optimal pretension of the spring. The optimization outputs 10 coefficients of which one is an offset and the other 9 are for the minimum angle of the motion, the maximum angle of the motion, the speed, and the combinations between them, as can be seen in equation 1. These values are used in the mapping on the suit controller, which using the IMU, then generates the desired pretension.

$$d_{\text{pretension}} = c_1 + c_2\theta_{\min} + c_3\theta_{\max} + c_4\omega + c_5{\theta_{\min}}^2 + c_6{\theta_{\max}}^2 + c_7\omega^2 + c_8\theta_{\min}\theta_{\max} + c_9\theta_{\min}\omega + c_{10}\theta_{\max}\omega \quad (1)$$

The user study consists of four experiments, designed to show the performance in different operating modalities. During the experiments, the participants were shown an animation of the skeleton used in OpenSim, moving the arm in a variety of elevation ranges and speeds, as depicted in figure 2, which they were asked to track as best they can.

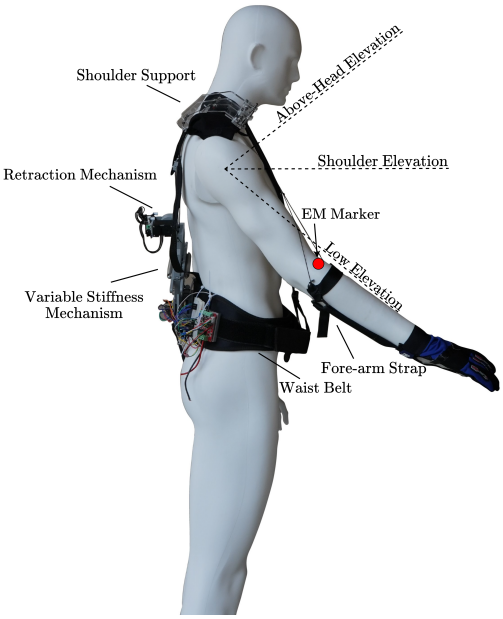

Fig. 2: The exosuit used in the user study with the addition of the variable stiffness mechanism to illustrate the elevation ranges of the experiments in the user study. Additionally, the location of the EM marker used to illustrate arm elevation is indicated by the red marker.

The four experiments are as follows:

1) Experiment 1: The first experiment consists of an oscillating motion of constant speed in three ranges, lower elevation, shoulder elevation, and above-head elevation. Each of the sections consisted of 10 cycles as seen in figure 3.

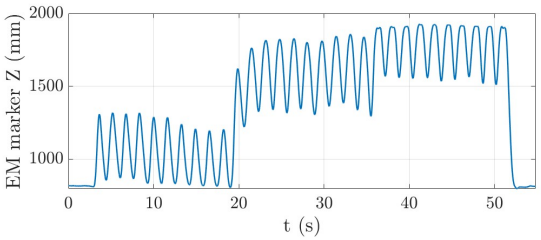

Fig. 3: The Z position of the EM marker placed on the inner protruding bone of the elbow of participant 5, for the first experiment of the user study.

2) Experiment 2: The second experiment is to study the effect of the angular velocity of the motion on the muscle effort reduction. The reference trajectory is an oscillating motion at shoulder elevation, again consisting of three sections, each 10 cycles. The first section would be the normal movement speed, the second slightly slower, and the last section faster than the first, as illustrated in figure 4.

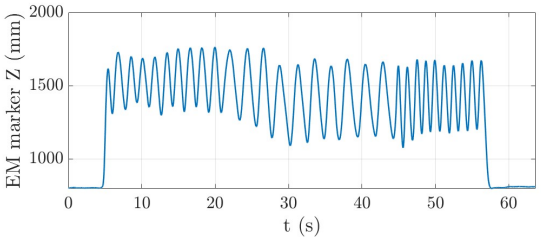

Fig. 4: The Z position of the EM marker placed on the inner protruding bone of the elbow of participant 5, for the second experiment of the user study..

3) Experiment 3: In the third experiment, the participant is given a 2 kg weight to accentuate the muscle effort reduction and is asked to track an oscillating motion at shoulder elevation for 10 cycles, seen in figure 5.

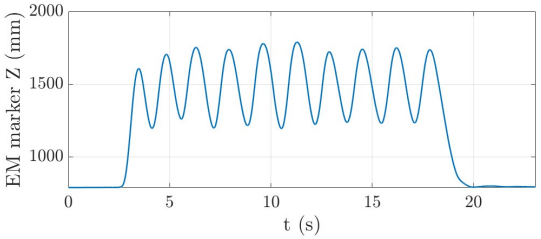

Fig. 5: The Z position of the EM marker placed on the inner protruding bone of the elbow of participant 5, for the third experiment of the user study..

4) Experiment 4: In the fourth and last experiment, the participant is again given a 2 kg weight and is asked to track an oscillating motion now at an above-head elevation for 10 cycles, as seen in the greater Z position in figure 6 compared to figure 5 .

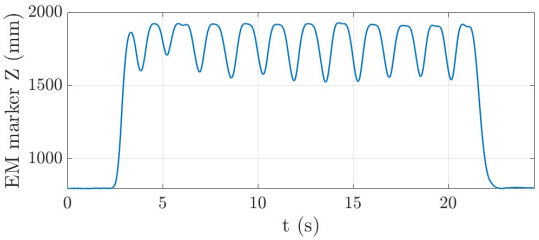

Fig. 6: The Z position of the EM marker placed on the inner protruding bone of the elbow of participant 5, for the fourth experiment of the user study..

A. Results

These experiments are performed while measuring the electromyography, or EMG, of the Anterior, Mid, and Posterior Deltoid, in addition to the Trapezius. The participant is also equipped with a wide set of tracking markers to measure the position of various skeletal landmarks and the position of suit elements, which could be used in the previously mentioned musculoskeletal simulation program, OpenSim, to compare the simulation to the measurements.

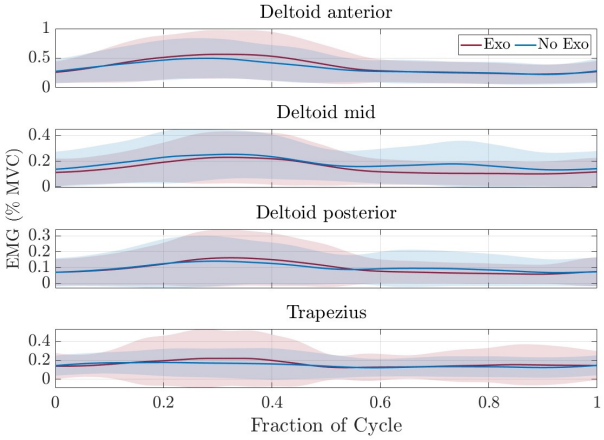

Fig. 7: The measured EMG data from experiment one for all muscles over the fraction of that cycle.

The EMG measurements as a percentage of the maximum voluntary contraction, MVC, can be seen in figure 7, 8, 9, and 10, over the fraction of the cycle. The cycles are automatically extracted from the various experiments, filtered to eliminate outliers, and selected based on the exosuit being deemed active. The exosuit was said to be active if the error between the current motor position and the desired motor position was less than 10 %, which would in terms of pretension equal at most a 0.14 mm error. If this requirement held for at least 90 % of the cycle, the cycle was added to the dataset.

The figures are best evaluated by looking at the mean of the EMG data, depicted as the solid line, and comparing

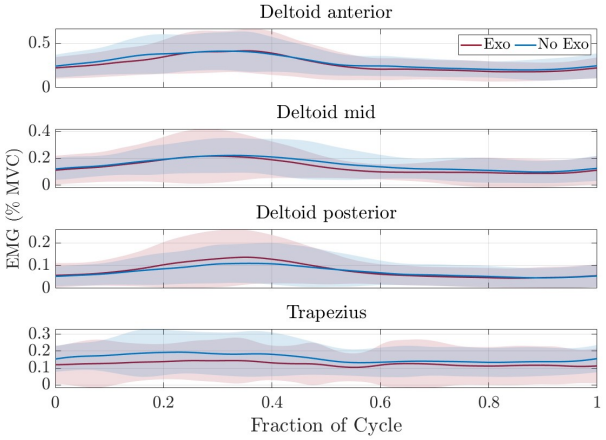

Fig. 8: The measured EMG data from experiment two for all muscles over the fraction of that cycle.

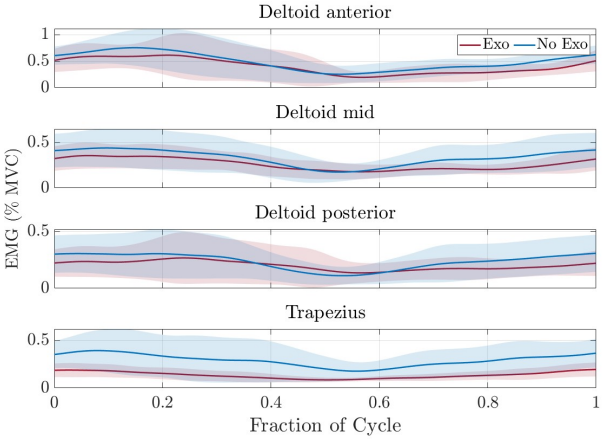

Fig. 10: The measured EMG data from experiment four for all muscles over the fraction of that cycle.

the exosuit condition to the no exosuit condition. Of note is that the EMG reduction, the difference between the no exosuit condition and the exosuit condition, differs between the experiments and muscles. This illustrates the areas in which the exosuit is most effective or possibly even requires a higher muscle effort.

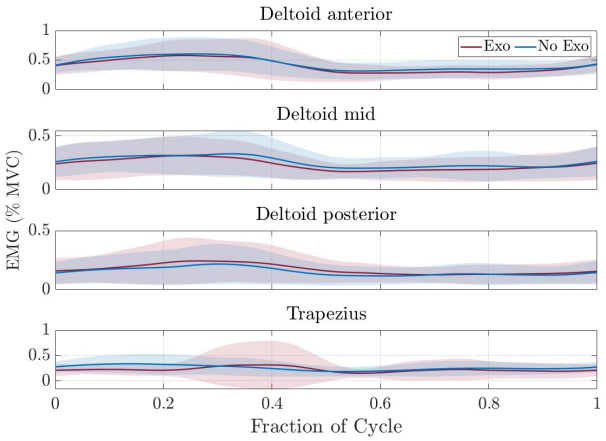

Fig. 9: The measured EMG data from experiment three for all muscles over the fraction of that cycle.

Experiment 4, depicted in figure 10, for instance, shows a reduction in all muscles for the majority of the cycle which strengthens the reasoning for the suit, as it was primarily designed to reduce the muscle effort in overhead motions. Additionally, as previously mentioned, the participant is holding a 2 kg weight, which helps to highlight improvements between the exosuit and no exosuit condition as the added weight requires greater muscle activation and accelerates the onset of muscle fatigue.

There exist also experiments that showed an increase in the EMG measurements, like experiment 1 as seen in figure 7. Here there is a clear increase for the Deltoid anterior, and Trapezius, with a decrease in the muscle effort only for the Deltoid mid and the Deltoid posterior. This could be due to the lower effectiveness of the exosuit in the lower range due to the cable wrapping over the shoulder for a greater angle compared to at greater elevations of the arm.

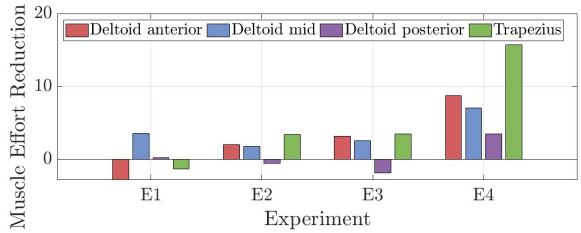

Fig. 11: The mean percent muscle effort reduction for each experiment and muscle.

Figure 11 can be used to better evaluate the inter-experiment EMG reduction between the no exosuit condition and the exosuit condition. A positive percentage correlates to lower measured EMG activity in the corresponding muscle for the exosuit condition. To reiterate, the suit was initially designed to assist in overhead motions in which it seems to excel based on the high muscle effort reductions seen in all muscles for experiment 4.

B. Discussion

Figure 11 clearly illustrates the reduction in muscle effort for the majority of muscles and experiments using the exosuit. During the user study, there were however moments when the participants expressed discomfort due to the pretension in the cable leading to the cable pressuring the shoulder, especially evident in lower arm elevations due to the cable wrapping over the shoulder.

The suit would occasionally also be required to extensively pretension the spring, causing the participant's arm to be forcibly raised, possibly to an uncomfortable elevation. This is due to the system only being able to control the pretension of the spring and thereby moving the equilibrium position to attain the desired assistive force. The addition of a variable

stiffness actuator having the ability to control the equilibrium position and the effective stiffness would prevent such scenarios, as in order to achieve greater forces, the stiffness could be increased without moving the equilibrium position. This would hypothetically prove most effective for movements within a small range, such as experiment 4, where the stiffness could be set extremely high and with the equilibrium position being close to the movement range. It might also prove beneficial for static scenarios, in which case the stiffness could be set to infinite so as to completely support the arm of the wearer, maximally reducing the muscle effort.

Additionally, as the effectiveness of the suit has been illustrated, the user study and the accompanying work are being prepared to be published.

III. Design Specifications

Section II showed the effectiveness of the exosuit capable of only pretensioning a spring and highlighted theorized benefits of a variable stiffness actuator if used in the suit. This section thus outlines the design requirements that stemmed from the user study, and in doing so bounds the solution space. The mechanism itself will be designed with the preferred location being on the lower back as this is the same location the previous mechanism was placed during the user study, where it proved a convenient location for donning and doffing the suit as well as bearing the load of the mechanism by attaching it to a big belt as seen in figure 28.

A. Functional Requirements

1) Maximum Tension: The mechanism will be designed to function within the same operating conditions as the previous generation suit used in the user experiments. The suit utilized two springs in parallel with a total stiffness of $425\,\mathrm{N/m}$. The desired pretension length of the spring measured during the user study was up to $231\,\mathrm{mm}$ with the maximum measured deflection of the spring being $163\,\mathrm{mm}$. This combined with the previously mentioned spring stiffness results in a maximum force of $69\,\mathrm{N}$ measured during the user study. Considering a safety margin of at least 10% the designed for maximum force is chosen to be $80\,\mathrm{N}$.

2) Stiffness Range: In the user study, the stiffness was chosen from the following set of available stiffnesses: $74\,\mathrm{N/m}$, $132\,\mathrm{N/m}$, $254\,\mathrm{N/m}$, $329\,\mathrm{N/m}$, $425\,\mathrm{N/m}$, and $490\,\mathrm{N/m}$. The $425\,\mathrm{N/m}$ stiffness was chosen due to a higher stiffness requiring less pretensioning of the spring and due to the estimated maximum travel of the spring located on the upper arm. The to-be-designed mechanism should at least be capable of reaching the stiffness used in the user study to allow for a conclusive comparison and would preferably also be able to become completely compliant to the wearer for safety reasons. Being able to additionally set the mechanism to an infinite stiffness might also be desired as it would allow the user to hold their arm stationary with the mechanism bearing the majority of the load. The to-be-designed for stiffness range thus will be from $0\,\mathrm{N/m}$ to $\infty\ \mathrm{N/m}$.

3) Retraction Distance: As previously mentioned, the highest desired pretension during the user study was $231\,\mathrm{mm}$, but that is also due to it having to pretension the springs, as well as account for the change in equilibrium position. In order to obtain an estimate of the distance the mechanism has to actuate to move the equilibrium location of the total system, a wire was attached to the forearm and routed over the right shoulder to the center of the lower back where the position of the wire was marked at the top of the belt. The arm was first placed vertically up as this would be the maximum elevation of the arm, after which the arm would be completely lowered to be pointing down so that the error between the two could be determined. Measuring on an $180\,\mathrm{cm}$ male resulted in a measured distance of approximately $160\,\mathrm{mm}$. Considering taller people, or those with larger shoulders, a maximum retraction distance of $200\,\mathrm{mm}$ is chosen as the to-be-designed for value. Noteworthy is that the $160\,\mathrm{mm}$ retraction corresponds to a 180-degree rotation of the arm, illustrating the large effect a small displacement of the mechanism has on the arm angle.

B. Performance Criteria

1) Speed: The mechanism should be able to actuate the previously mentioned retraction distance in 2 seconds or less as this is approximately the time it takes to lift the arm from minimum to maximum elevation. A stiffness change from $0\,\mathrm{N/m}$ to $\infty\ \mathrm{N/m}$ should also be able to be done within this same time window.

2) Weight: The weight of a portable solution is crucial for the comfort of the user and should thus be kept to a minimum or allocated such as to optimize for the comfort of the wearer.

3) Power Consumption: Another crucial metric in a portable solution is power consumption as this will, combined with the desired operating time, result in the required battery capacity of a system equipped with the variable stiffness actuator, adding additional weight. The average power consumption of the system should therefore be kept to a minimum.

4) Inertia: The inertia of the mechanism should be as low as possible to maximize the transparency to the user and minimally affect the bandwidth of the motions.

C. Wishes

The mechanism would preferably be affordable to build to allow anyone to easily recreate it as the linear variable stiffness mechanism can be used in other settings also. Additionally, the design should be easily manufacturable with limited resources as this would further promote easy replication and improvement of the design both during the design phase and beyond.

Furthermore, the center of mass of the mechanism should be kept as close to the back of the wearer as possible to minimize the generated moment due to gravity, improving the comfort.

IV. System Design

Most of the variable stiffness designs found in the literature phase are for rotary joints with only one being designed for a linear motion but was still applied in a rotary joint [29]. With that in mind, a point of reference remains valuable to

compare existing variable stiffness solutions for rotary joints to understand the capabilities of current solutions.

TABLE I: Exemplary variable stiffness joints

Name	VS-Joint [11]	DLR FSJ [14]	vsaUT-II [21]	AwAS-II [20]
Max.Torque	160 Nm	67 Nm	60 Nm	80 Nm
Max. Stiff.	55 Nm/deg	83.7 Nm/deg	16.5 Nm/deg	∞ N/deg
Zero Stiff.	✗	✗	✓	✓
Max. Defl.	$\pm 14°$	$\pm 15°$	$\pm 20°$	$\pm 17°$
Weight	1.4 kg	1.41 kg	2.5 kg	1.1 kg

It is challenging to compare these systems to the to-be-designed system due to the target application being linear as opposed to rotation and would benefit from a greater deflection at a lower stiffness. Noteworthy, however, is the fact that only two of these actuators have the capability to be completely compliant, namely the vsaUT-II actuator by [21] and the AwAS-II actuator by [20], with only the latter having the ability to also become completely rigid. A further limitation within these designs is the limited deflection angle of the joints, which for their designed purpose is most likely ideal, but would translate poorly if used in a linear mechanism using a pulley due to the previously mentioned preference for greater deflections at a lower stiffness.

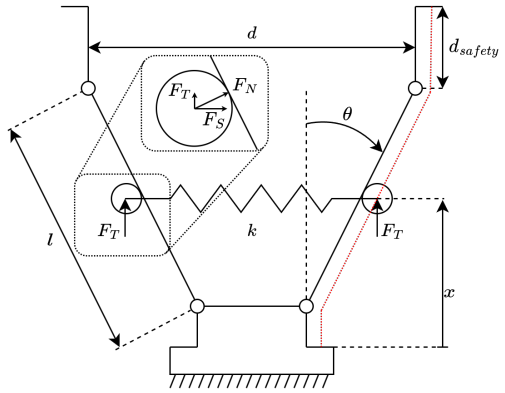

Fig. 12: Concept of the variable stiffness mechanism with the angle θ of the slope as the controlled variable. Two bearings roll over the surface along the red-dotted path and exert a normal force F_N on the surface which can be decomposed into F_S and F_T at a displacement of x. Between the two bearings, a spring with stiffness k_s is placed that extends as the bearings further separate, increasing F_S and thus F_T. The distance d_{safety} has been added as a short piece that has an output stiffness of only $4.4\,\text{N/m}$ in the event that there is an excessive amount of force on the mechanism in the lower operating stiffness range.

A. Variable Stiffness

The variable stiffness mechanism is designed to adhere to the requirements set in section III. The specific application of the exosuit allows freedom due to the absence of the usual constraint given to the variable stiffness mechanisms seen in the literature, namely that it has to be as compact as possible to fit in a joint. The variable stiffness mechanism will be placed on the lower back where there is ample space in the plane parallel to the back. As mentioned in section III-C, the center of mass should be kept as close to the back as possible which can be achieved by minimizing the mechanism thickness.

The working principle of the developed concept can be seen in figure 12, where the angle θ can be adjusted using a motor. The system has two bearings that roll over the surface and follow the red-dotted line and are each bearing a tension F_T at a displacement of x. As the slope increases, the rate at which the spring extends with an increase of displacement x also increases and thus the output stiffness increases. The mechanism effectively multiplies the stiffness of the spring using mechanical advantage, and can thus be categorized under the structure-based variable stiffness mechanisms as discussed in section I.

After conceptualizing the functionality of this mechanism, a design was found that utilized a similar working principle to obtain a nonlinear stiffness by having the bearings roll over a nonlinear surface, and in doing so map linear springs to any nonlinear spring output for use in an antagonistic-based variable stiffness mechanism [16]. The main difference between the presented concept and the found design is that the concept will be able to adjust the spring characteristic during operation and the found design has no such ability as the profile has to be manufactured in advance.

$$F_S = k \cdot s = k_s 2x \tan(\theta) \tag{2}$$

$$F_T = \tan(\theta) F_S = k_s 2x \tan(\theta)^2 \tag{3}$$

$$F_{\text{Total}} = 2F_T = k_s 4x \tan(\theta)^2 \tag{4}$$

$$k_{\text{output}} = \frac{F_{\text{Total}}}{x} = k_s 4 \tan(\theta)^2 \tag{5}$$

$$\theta = \text{atan2}(\sqrt{k_{\text{output}}}, \sqrt{4k_s}) \tag{6}$$

In the configuration where θ is zero, the mechanism will have an output stiffness of $0\,\text{N/m}$ as there is no extension of the spring. Then, as θ increases, the output stiffness will increase with x and θ as defined by equation 5. The top plot in figure 13 illustrates the output stiffness k_o as a function of θ for three available spring stiffnesses. This stiffness would continue to increase until infinity at $\theta = 0.5\pi$.

As the mechanism is able to theoretically create any output stiffness from an input stiffness, the spring stiffness k_s needs to be chosen based primarily on the desired granularity of the output stiffness and the maximum output deflection. A lower spring stiffness allows for greater control in the lower stiffness range however also requires a greater angle θ to obtain higher output stiffnesses and thus limits the possible extension of the mechanism in the higher stiffness range. At greater angles of θ the maximum range over which the mechanism can operate decreases as can be seen in the bottom plot in figure 13, which illustrates the relation between θ and the maximum possible extension of the mechanism $x_{\max}$.

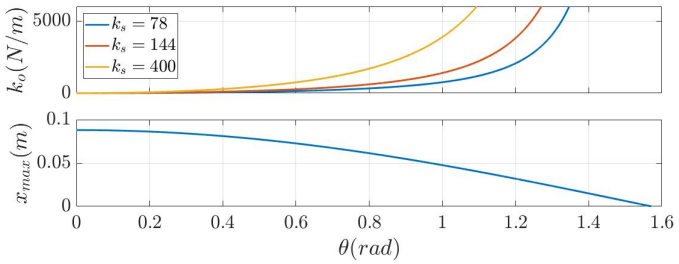

Fig. 13: The top plot illustrates the relation between the spring stiffness k_s, θ, and the output stiffness k_o. The bottom plot gives the relation between the spring stiffness θ and the maximum extension of the mechanism $x_{\max}$.

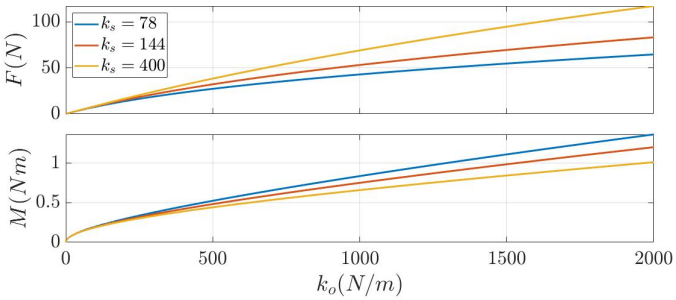

Fig. 14: The top plot illustrates the relation between the output spring stiffness k_o, and the required force to trigger the safety F. The bottom plot shows the relation between the output spring stiffness k_o, and the required moment M to actuate one arm at the maximum chosen arm length of $88\,\mathrm{mm}$.

A spring stiffness of $144\,\mathrm{N/m}$, consisting of two $72\,\mathrm{N/m}$ springs in parallel, was chosen from the set of available springs as the lower stiffness would allow for greater control in the lower stiffness range while also having an outside diameter of $12.5\,\mathrm{mm}$ with a rest length of $76\,\mathrm{mm}$, making it ideal for the mechanism to remain thin while increasing in width along the back.

The addition of the $4.4\,\mathrm{N/m}$ section of length d_{safety} was added based on experience from the user study discussed in section II, as occasionally, the wearer would experience a higher than comfortable tension and thus would be forced to lift the arm practically vertical. The reason the stiffness is nonzero is that the low stiffness still generates enough force to reset the mechanism. The distance d_{safety} would theoretically allow for the mechanism to be overpowered as long as it would be operating a stiffness range that would not require an impossible amount of force. The distance d_{safety} can be quite short since a small displacement would have a large effect on the arm angle as discussed in III-A3.

Figure 14 illustrates the relation between the output stiffness and the required force to trigger the safety with the mechanism having an arm length l of $88\,\mathrm{mm}$. For the previously mentioned spring stiffness of $144\,\mathrm{N/m}$ the required force at an output stiffness of $2000\,\mathrm{N/m}$ would theoretically be $83.2\,\mathrm{N}$. This is slightly higher than the maximum force, as set in III-A1, ensuring the maximum force can still be achieved. A greater force would trigger the safety, which could be modified by either altering the length of the arms or the desired output stiffness. The addition of the safety does complicate the design somewhat since it requires the design to function as a parallelogram to ensure the stiffness at the end remains $4.4\,\mathrm{N/m}$.

The maximum required moment M to actuate with an arm length of $88\,\mathrm{mm}$ as a function of the output stiffness relation k_o can be seen in the bottom plot of figure 14. At an output stiffness k_o of $2000\,\mathrm{N/m}$, the maximum required moment to actuate one arm is $1.2\,\mathrm{Nm}$, thus the total moment required to actuate both arms is $2.4\,\mathrm{Nm}$. The system uses a motor that was already available in combination with a worm wheel to make the system non-back-drivable and thus reduce the energy consumption of the system. The motor has a rated operating torque of $0.125\,\mathrm{Nm}$ with a peak torque output of $0.38\,\mathrm{Nm}$ [30] and is combined with an also already available worm wheel that has a 90:1 reduction ratio [31]. Furthermore, the axis of the worm wheel is fitted with a magnet and an as5600 hall sensor [32] to provide feedback to the controller.

The system, additionally, has another transmission ratio due to the differing diameters of the pulley on the worm wheel being $32.3\,\mathrm{mm}$ and the diameter of the pulley on the arm being $68\,\mathrm{mm}$ as seen in figure 16a, resulting in a ratio of 1.98:1. This subsequently leads to a total reduction ratio of 178.2:1, leading to a maximum peak operating torque of $22.275\,\mathrm{Nm}$. This is many times greater than the required torque at an output stiffness k_o of $2000\,\mathrm{N/m}$, and would theoretically allow the system to actuate at a maximum displacement for a stiffness of $40\,000\,\mathrm{N/m}$. The reason for using wires rather than direct gearing was that it would allow for easy symmetrical actuation due to the absence of play in gears and improve efficiency as there is no sliding contact.

With the previously mentioned total reduction ratio of 178.2:1 and the nominal speed of the motor being $4000\,\mathrm{rpm}$ [30] the motor could theoretically actuate $2\,\mathrm{s} \cdot 360\,\mathrm{deg} \cdot \frac{4000\,\mathrm{rpm}}{60\,\mathrm{s}\cdot 178.2} = 269.36\,\mathrm{deg}$ in two seconds. This would satisfy the performance criteria set in section III-B1.

To maintain a slim design, the decision was made to mount two springs on the outside of the mechanism, cutting down on the amount of structural material needed due to only a single guiding mechanism having to be located in the center as opposed to one on each side. The additional benefit is that springs with a similar rest length could be easily exchanged. The guiding mechanism, consisting of two bearings rolling over the inner surface as seen in figure 16a, ensures the mechanism remains in the correct orientation under a possibly asymmetrical load. This is also the reason for the two attachment points on the carrier as this causes it to self-align under load. The design of the variable stiffness mechanism can be seen in figure 15.

B. Rest Length Adjustment

Now the variable stiffness element of the mechanism has been designed, a mechanism needs to be designed to reduce

Fig. 15: The last iteration of the variable stiffness mechanism device without a rest length adjustment mechanism.

the cable length. The biggest challenge is creating a design that integrates well with the variable stiffness mechanism while adhering to the requirements. To this extent, to maintain the possible deflection of the integrated solution, the existing cable layout has to be modified in order to maintain the 1:1 movement of the output to the mechanism using a pulley as seen in figure 16a and figure 16b.

The first iteration of the design can be seen in figure 16b where a servo is used to rotate a pulley to spool the cable. Due to the cable layout, the cable retraction mechanism has to actuate twice the distance for the desired output retraction distance. At the maximum force set in III-A1 and with a pulley diameter of $40\,\mathrm{mm}$ the required torque is $0.8\,\mathrm{Nm}$, not accounting for any friction or losses in the system. A Dynamixel XM-430-r was chosen as it was available, easy to use, and has a rated stall torque $3.0\,\mathrm{Nm}$ at $12\,\mathrm{V}$ [33], in addition to allowing for continuous rotation. It has to be emphasized that this is but the first iteration of the design and currently does adhere to the performance requirement as set in III-B1, as with a $40\,\mathrm{mm}$ pulley, the system would need $2.48\,\mathrm{s}$ to actuate $0.2\,\mathrm{m}$ without load. The pulley diameter could be increased but doing so would result in a lower output force, which was prioritized for this design iteration. Additionally, The current design requires the servo to continuously actuate and thus does not optimize the performance requirement as set in III-B3. Ideally, a similar non-backlash system, such as a worm wheel, would be used to allow for minimal actuation. The design could be effectively improved by using a different actuation solution that would also allow for continuous rotation while having a higher rated torque while including a non-backlash solution as will be further discussed in section VII.

C. Integrated Design

The last step of the design process integrates the variable stiffness mechanism with the cable retraction mechanism. The variable stiffness mechanism was designed first, with the cable retraction mechanism being designed with that in mind, connecting to the guide structure using a set of bolts as illustrated in figure 16b. The design including the control electronics weighs $1224\,\mathrm{g}$ which is comparable to the designs presented in table I. A large part of the weight is due to the stiffness actuation motor weighing $0.45\,\mathrm{kg}$ [30], and as previously mentioned was chosen for availability and will be further discussed in section VII.

D. Control

The chosen controller is a PI controller as the target application is reference tracking, allowing for a minimal steady-state error. A block diagram of the controller can be seen in figure 17. The controller was manually tuned through trial and error, most likely limiting the performance of the controller, but being considered sufficient for this work. The reference angle of the worm wheel r is set based on the desired stiffness as defined in equation 6 that is derived from equation 5. The error e between the measured angle of the worm wheel y and r is then used as input of the PI controller which outputs the motor velocity that accepts a range from 0, being zero velocity, to 4095, being the maximum motor velocity. The integral in the PI controller is saturated at a value of ± 250 to allow for fast changes in direction and little overshoot, while the control input is bounded to a value of 1500 to limit the speed of the system. Once the system has been thoroughly tested this could be increased to allow for a faster stiffness change or to further increase the ability to change stiffness when force is applied to the system.

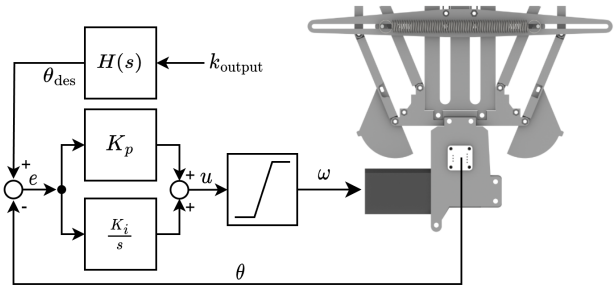

Fig. 17: Block diagram of the system with k_{output} being the desired output stiffness, which is then transformed to a resulting desired motor angle θ_{des} using equation 6 in combination with the transmission ratio between the arms and the worm wheel. The error e between the desired angle θ_{des} and the measured angle of the worm wheel θ, is used as an input in the PI controller. u is the control input determined by the PI controller which is the motor velocity from stationary being 0 to the maximum velocity being 4095 and is bounded to limit the speed of the system.

V. Experiments

Experiments were performed throughout the iteration process to debug and validate the code and mechanical design. After the most recent iteration of the mechanical design, it was decided to redo all tests while externally measuring the position of a series of markers placed on the design as illustrated in figure 18 using an OptiTrack system. The reasoning behind

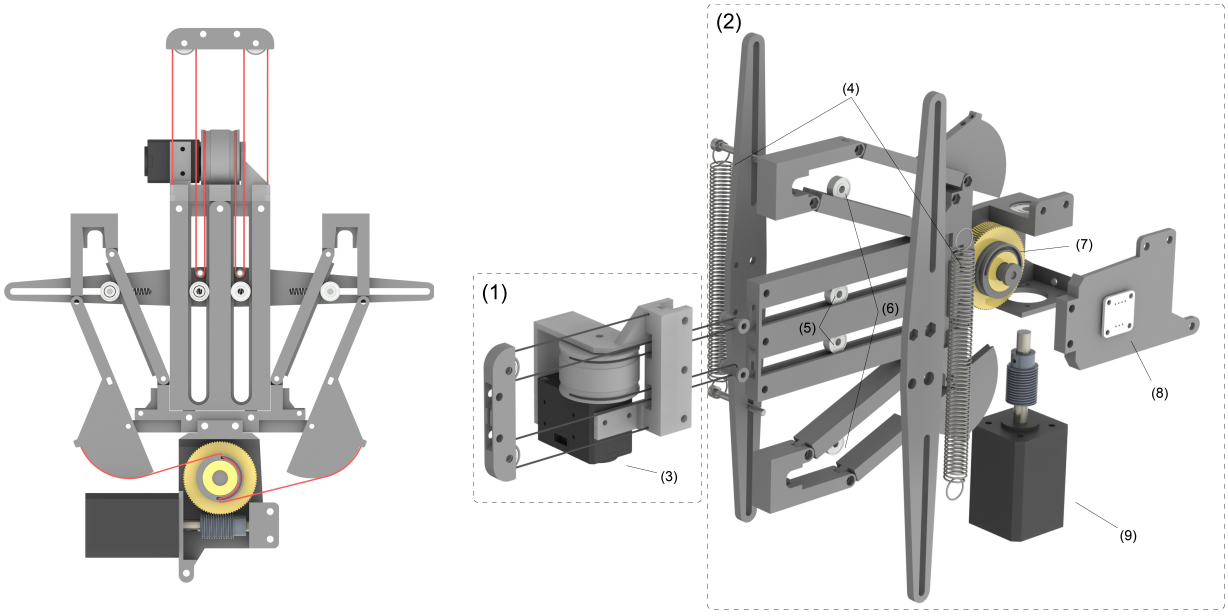

(a) (b)

Fig. 16: (a) A top-down section view illustrating the cable routing of the mechanism in red and the mechanism of actuation for the arms. (b) An exploded view of the mechanism highlighting the most important components. (1) The retraction mechanism mainly consists of (3) the retraction servo. (2) The variable stiffness mechanism with (4) the two springs, (5) the guiding roller bearings, (6) the roller bearings for the springs, (7) the worm wheel with integrated pulley, (8) the hall effect sensor, and lastly (9) the motor for the stiffness actuation.

this decision was that higher than expected deformation of the mechanism was observed and the loadcell reading would fluctuate more than expected over time. The tracking markers would enable the validation of the mechanism configuration and could be used to determine the deflection under load.

To validate the functionality and performance of the design a series of experiments were performed:

- Repeatability
- Constant displacement
- Constant force
- Limit test
- Performance analysis
- Bending analysis

A. Methodology

For all the experiments, the OptiTrack system was set to sample at 200 Hz while the data from the Teensy microcontroller would stream at 10 Hz over the serial communication bus to the terminal. The mechanism would be turned on and calibrated to the zero stiffness position based on the observed tension in the cables connecting the motor pulley to the arms. The mechanism would then be enabled, after which the OptiTrack system recording would be started. Depending on the experiment, the automated test or manual testing would commence. After the experiment finished, the Teensy data would be saved and the OptiTrack recording would be stopped. These were then aligned and trimmed to the same length of time after which the Teensy data is supersampled to match the sampling frequency of the OptiTrack recording allowing for easy data analysis using Matlab.

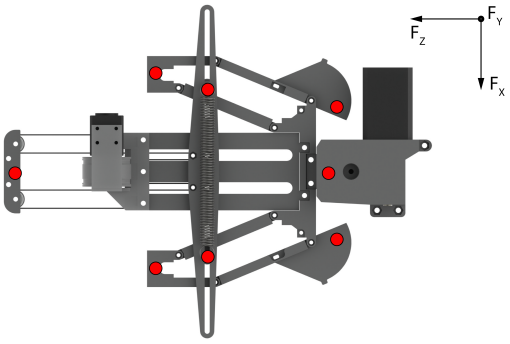

Fig. 18: Marker placement on the mechanism for the experiments.

B. Repeatability

To validate the repeatability of setting the mechanism stiffness a test was performed where the mechanism stiffness would increase with $50\,\mathrm{N/m}$ increments and be pre-tensioned with a distance of Δx_p m, as defined by equation 7. The pretension distance Δx_p is near the limit of the mechanism before the safety would be triggered. This was done over a range from $50\,\mathrm{N/m}$ to $2000\,\mathrm{N/m}$ as this was found to be the range in which the retraction mechanism was able to actuate consistently. Frames of one of the experiment trials

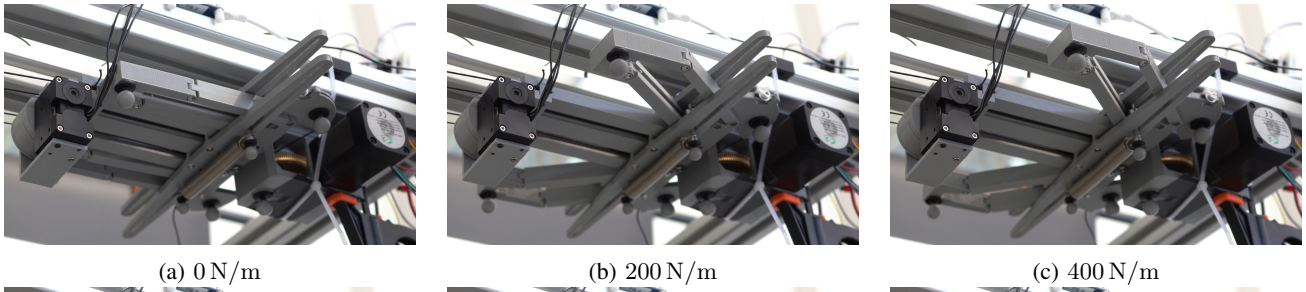

(a) $0\,\mathrm{N/m}$ (b) $200\,\mathrm{N/m}$ (c) $400\,\mathrm{N/m}$

(d) $800\,\mathrm{N/m}$ (e) $1600\,\mathrm{N/m}$ (f) $2000\,\mathrm{N/m}$

Fig. 19: Frames taken from the repeatability experiment with increasing stiffness from (a) to (f). It illustrates well the nonlinear relation between the desired output stiffness and the angle θ of the arms.

can be seen in figure 19. This test was performed 13 times without adjusting the output position of the system but with re-calibration of the initial position after each experiment. There was some slack in the output cable in the starting position meaning the mechanism would in reality actuate slightly less than Δx_p m which was compensated for using the measured -position of the tracking markers.

$$\Delta x_p = 2 \cdot 0.088 \cos(\theta) \tag{7}$$

Due to the complete data collection, various methods of calculating the resulting stiffness are possible of which two were chosen for their logic and hypothesized quality of data.

1) Calculated Stiffness Using Measured Force: The first method uses the force of the loadcell in combination with the measured displacement of the spring mechanism over the Z-axis as defined in figure 18, of which the results can be seen in figure 20. Figure 20 also illustrates the error between the desired stiffness and the calculated stiffness, showing an average stiffness error over all trials of this experiment of $-237.018\,\mathrm{N/m}$, meaning the mechanism was on average less stiff than desired. Furthermore, an increased variance can be seen as the desired output stiffness increases.

2) Calculated Stiffness Using Measured Spring Extension: The second method to calculate the stiffness is using the two markers on the springs to measure the spring extension by taking the Euclidean distance between the two points, multiplying that by the total spring stiffness of $144\,\mathrm{N/m}$, and using the relation in equation 3 in order to calculate the resulting output force. This force is divided by the displacement of the spring in the Z-axis, like in the other method, and results in an output stiffness as can be seen in figure 21. The average stiffness error k_e over all trials in this experiment was found to be $-306\,\mathrm{N/m}$ which indicates the mechanism was on average

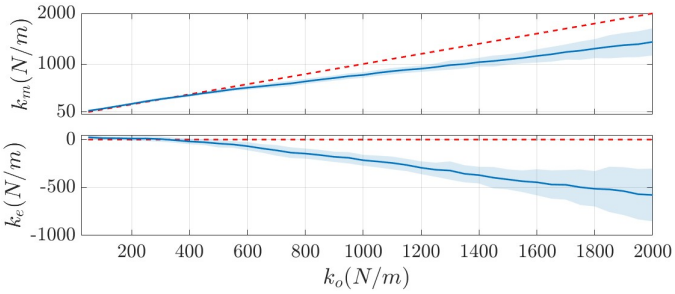

Fig. 20: The top plot shows the relation between the measured output stiffness k_m, calculated using the measured tension and the displacement of the spring in the Z direction as defined in figure 18, against the target output stiffness k_o. The bottom plot shows the stiffness error k_e between the measured stiffness and the desired output stiffness.

over all the experiments below the desired stiffness using this method.

3) Comparison Of Methods: As seen, the two methods for calculating the stiffness result in quite different values. The second method has a closer grouping of the stiffnesses compared to the first method, possibly due to the varying output of the loadcell. Additionally, the range of the error is smaller in the second method with a maximum standard deviation of $266.94\,\mathrm{N/m}$, as opposed to from $308.79\,\mathrm{N/m}$ for the first method.

In both of the methods, the effect of the system compliance can be seen in the figures as the error grows larger due to the higher angle and force, further studied in section V-G. Effectively, this would equate to two springs in series, that being the actual springs and the mechanism itself, leading to a lower output stiffness. Additionally, the force measurement

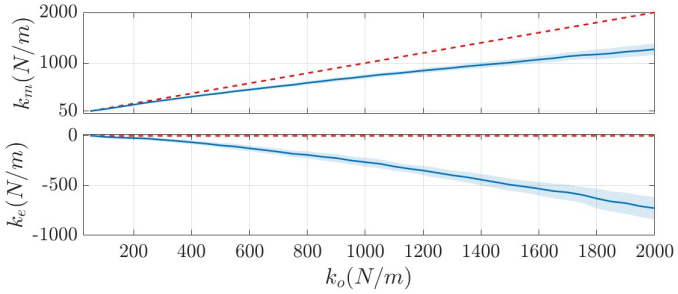

Fig. 21: The top plot shows relation between the measured output stiffness k_m, calculated using the measured extension of the spring, the motor angle, the force relation in equation 3, and the displacement of the spring in the Z direction as defined in figure 18, against the target output stiffness k_o. The bottom plot shows the stiffness error k_e between the measured stiffness and the desired output stiffness.

used in the first method seemed to fluctuate, making conclusions increasingly challenging.

This same repeatability study was performed with an older version of the cable retraction mechanism, where it was tested until $500\,\mathrm{N/m}$, showing a similar error in magnitude to the current experiment results for the range up to $500\,\mathrm{N/m}$. The larger observed error for the stiffnesses higher than $500\,\mathrm{N/m}$ was as such not recorded during the previous experiment and could be due to the inaccuracy of the mechanism to actuate to the exact required angle, as the difference in the angle for a constant increase in stiffness decreases at higher stiffnesses as described in equation 6.

The second method was chosen as the default method based on the observed inconsistency of the load cell data and the lower variance of the collected data. The second method should better reflect the actual state of the system as the physical spring extension is used. A counter-argument to the second method is that it negates the effects of friction in the system which would be better represented by the load cell data.

C. Constant Displacement

The constant displacement experiment illustrates the ability of the mechanism to change the output stiffness for a constant displacement of the system. The output of the system was fixed to a rigid frame with the mechanism placed at a displacement of $0.03\,\mathrm{m}$. This would allow for the exploration of a large range of stiffnesses but does prevent the mechanism from reaching an infinite stiffness as this would require the output to move due to the radius of the bearing as discussed in V-D.

The results from the experiment are illustrated in figure 22, where both the desired stiffness k_d and the measured stiffness k_m, as per the method in V-B2, and the error between them are shown. During the experiment, it was observed that the mechanism was more capable of reaching the desired stiffness if the mechanism first returned to the zero stiffness configuration. This most likely is due to the insufficiency of the controller to converge to the desired stiffness under load in a sufficient time window. The increased difficulty of the mechanism to converge to the desired stiffness can be seen in the second half of the plot where the stiffness was increased in smaller increments. The error between the desired stiffness and the measured stiffness increases with an almost linear relation with an increasing desired stiffness. The error was lower for the same stiffness if the mechanism was first reset to the zero stiffness configuration, as evident by the lower error in figure 22.

The highest measured tension using the loadcell was $83.10\,\mathrm{N}$, at which point the mechanism was unable to further actuate with the current controller and the limit placed on the motor controller as mentioned in section IV-D. The calculated force based on the method from V-B2, resulted in a maximum force of $99.53\,\mathrm{N}$.

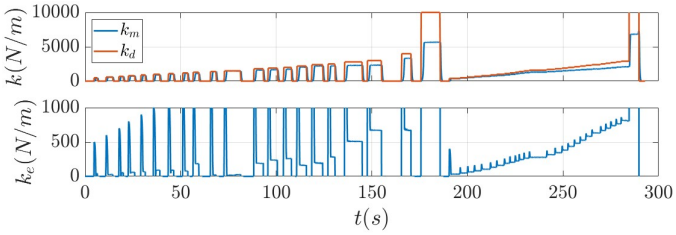

Fig. 22: The top plot shows the desired output stiffness k_d and the measured output stiffness k_m, as per the method in V-B2, over time for the constant displacement experiment. The bottom plot shows the error between the two over time.

D. Constant Force

To validate the ability of the mechanism to output a constant force, the mechanism has to counteract the change in force due to the stiffness change by Δx as defined by equation 9. As the stiffness, and thus the angle θ, is increased, there is a following displacement Δx_θ due to the offset of the center of the bearing with respect to the rolling surface. This relation is captured in equation 8, with θ_1 and θ_2 being the angles at a stiffness of k_1 and k_2 respectively.

$$\Delta x_\theta = r_{bearing}(\sin(\theta_1) - \sin(\theta_2)) \tag{8}$$

$$x k_{output,1} = (x + \Delta x + \Delta x_\theta) k_{output,2}$$

$$\Delta x = \frac{x k_{output,1}}{k_{output,2}} - x - \Delta x_\theta \tag{9}$$

Based on equation 9, an experiment was performed where the mechanism was set at an initial displacement of $0.03\,\mathrm{m}$ with an output stiffness of $400\,\mathrm{N/m}$ and then decreased with increments of $25\,\mathrm{N/m}$ to the final stiffness of $150\,\mathrm{N/m}$. Key frames of the experiment can be seen in figure 23. A lower stiffness would result in the mechanism safety triggering, as the required mechanism pretension would be greater than the actuation range. The results can be seen in figure 24, where the measured starting force was $11.85\,\mathrm{N}$ and ending with $8.99\,\mathrm{N}$ with a mean of $10.22\,\mathrm{N}$ and a standard deviation of $0.853\,\mathrm{N}$.

(a) 400 N/m

(b) 300 N/m

(c) 200 N/m

Fig. 23: Frames taken from the constant force experiment where the counteracting pretensioning can be seen in figures (a) through (c).

Figure 24 shows that the force is not quite constant during the experiment which most likely is due to the increase in the stiffness error as seen in the bottom plot. Additionally, the measured stiffness does not equal the desired stiffness, thus further influencing the result as the initial stiffness is used in equation 9 to determine the required retraction distance. The expected force with the mentioned starting stiffness and displacement would be 12 N, which is only slightly higher than the initial force measurement. Interestingly is how the system seems to stabilize after the stiffness is set to 300 N/m, after which it remains close to 10 N for the rest of the experiment.

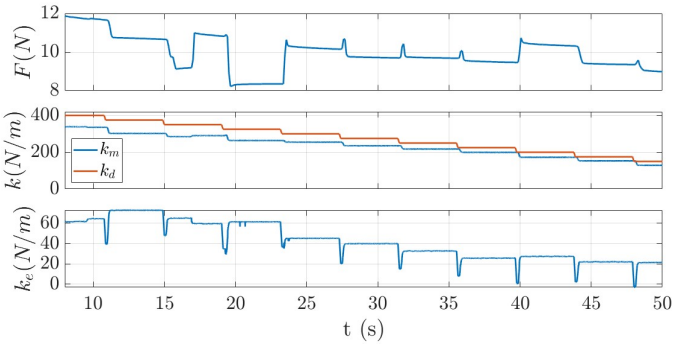

Fig. 24: The top plot shows the measured force from the loadcell F during the constant force experiment. The middle plot shows the desired output stiffness k_d and the measured output stiffness k_m as per the method described in V-B2. The bottom plot shows the error between k_d and k_m.

E. Limit Testing

In order to find the actual limits of the device including the pretensioning mechanism, a test was performed that would incrementally increase the mechanism stiffness and maximally pretension the mechanism with a distance of Δx_p m, as defined by equation 7. The results can be seen in figure 25. The stiffness at which the mechanism became unable to further actuate was at a desired stiffness of 2700 N/m with a measured stiffness of 1933 N/m at a peak force of 51.58 N. The reason the device was unable to further actuate was due to the error in the servo position being above the predefined limit. This limit could be increased at the expense of the output accuracy. With a force of 51.58 N, it does not satisfy the requirement set in III-A1 and should be further iterated upon as previously mentioned in section IV-B.

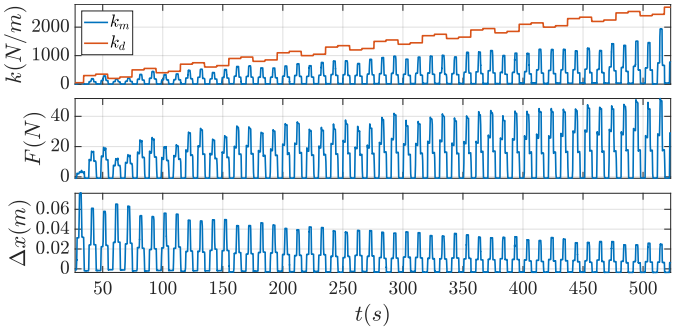

Fig. 25: The results of the limit test experiment.

F. Performance analysis

In order to validate some of the performance criteria, a test was done to find the capabilities of the mechanism to change the output stiffness from 0 N/m to ∞ N/m and from 0 N/m to 500 N/m. This experiment was performed without load to test the base capabilities of the mechanism. The mechanism

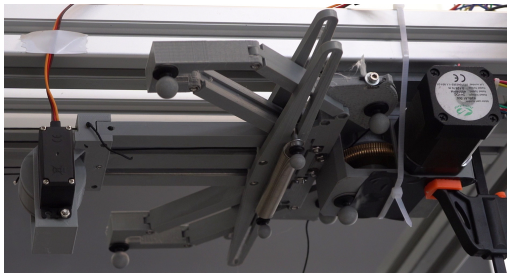

(a)

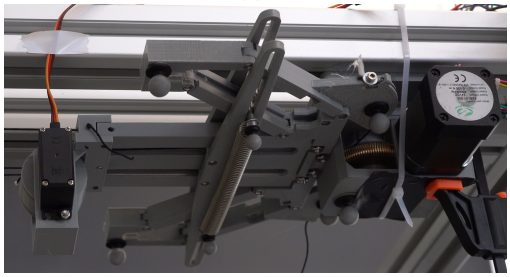

(b)

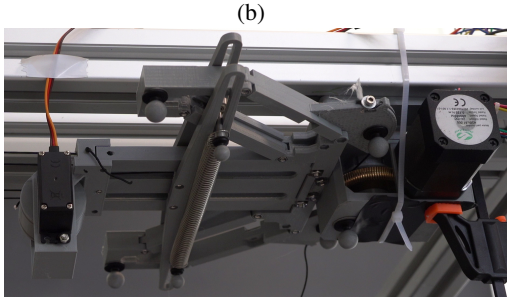

(c)

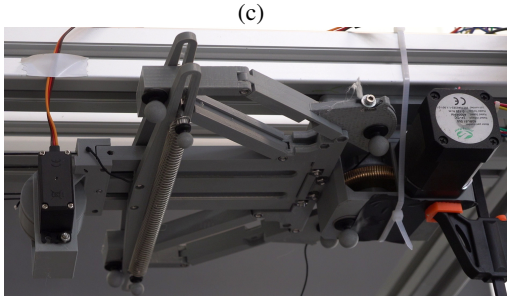

(d)

Fig. 26: The deflection experiment with frames (a) through (d) being of increasing force and deflection. The mechanism safety is triggered in figure (d).

was able to change stiffness from $0\,\mathrm{N/m}$ to ∞ $\mathrm{N/m}$ in $1.4\,\mathrm{s}$ and from $0\,\mathrm{N/m}$ to $500\,\mathrm{N/m}$ in $1.09\,\mathrm{s}$, thus complying with the requirement set in III-B1.

G. Deflection under load

As discussed in the introduction to this chapter, higher-than-expected deflection of the mechanism under load led to the experiments being performed using an OptiTrack system with markers being placed as seen in figure 18. Besides providing useful data on the spring displacement, it also allows for the measuring of the previously mentioned deflection of the mechanism. This was done by configuring the mechanism with a stiffness of $425\,\mathrm{N/m}$, chosen to match the stiffness from the previous user study.

The marker used for the analysis is the topmost marker in figure 18, as this element was observed to have the highest deflection under load. This can also be seen in figure 26, which shows frames from the experiment recording. The results of the experiment can be seen in figure 27, where a maximum deflection of $21\,\mathrm{mm}$ was measured when the mechanism was pulled into the safety and thus had the greatest moment generated. The average equivalent stiffness, meaning the force F divided by the displacement d, was on average $1835\,\mathrm{N/m}$ with a standard deviation of $1260\,\mathrm{N/m}$ and a maximum of $3834\,\mathrm{N/m}$ while under load. The measured deflection is still too high to be considered sufficient and will be further discussed in section VII.

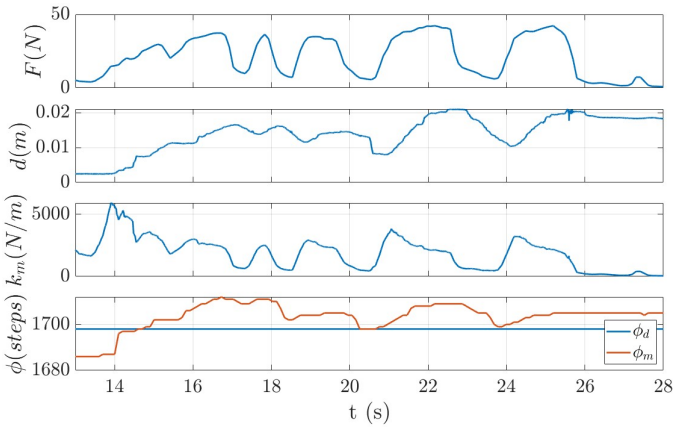

Fig. 27: The results of the bending analysis, from top to bottom: Measured force F, the Euclidean distance of the error of the uppermost marker as seen in figure 18, the equivalent stiffness based on the measured force and displacement, and the desired motor position ϕ_d and the measured motor position ϕ_m.

VI. Proof of Concept

To test the capability of the variable stiffness mechanism to be used in an exosuit, it was integrated into the suit used in the user study discussed in chapter II. The integrated suit fitted to a mannequin can be seen in figures 2 and 28.

The suit was also tested to verify the basic working principle by manually setting the stiffness and pretension as opposed to the biomechanically-aware optimization used in the user study. By pretensioning the system to an equilibrium position where the arm was elevated above the head, and subsequently testing multiple stiffnesses, it was found that there was indeed a significant difference in the stiffness of the mechanism and the effective level of support. The safety was also triggered multiple times in the experiment, showing the functionality of the safety mechanism. A frame from the experiment can be seen in figure 1.

One limiting factor in the efficacy of the design was the total system friction, meaning the friction in the suit itself

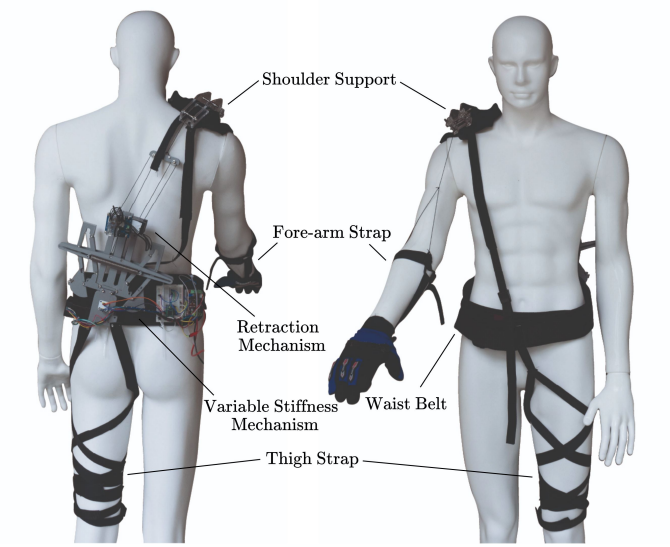

Fig. 28: Exosuit from the user study equipped with the variable stiffness mechanism.

combined with that of the variable stiffness mechanism, of which the first was already noticed in the user study. The suit and mechanism friction should be improved to ensure the functionality of the total design to do a follow-up user study to validate the hypothesis that the addition of the variable stiffness mechanism could further decrease the cumulative muscle effort.

VII. Discussion & Conclusion

This work showed a novel variable stiffness mechanism with a linear stiffness output designed for linear motion with intended use in an exosuit, developed because of a need stemming from a user study performed utilizing a passive-adaptive exosuit. A set of requirements and performance criteria were set including some design wishes, after which an overview is given of existing variable stiffness mechanisms designed for use in traditional joints. The design process was shown for both the variable stiffness mechanism itself and the retraction mechanism to pretension the system. Experiments were performed to test the validity and performance of the design as well as to explore any possible shortcomings. Finally, the developed solution was integrated into the exosuit used in the aforementioned user study, and tested as a proof of concept.

The experiments did indeed validate the working principle and functionality of the design and demonstrated the capabilities of using readily available linear springs and transforming them to any desired linear output stiffness. The variable stiffness mechanism was validated to be capable of sustaining the force requirement set, although a relatively high deflection at the end of the arms was measured highlighting a limitation of the current design and the need to further explore possible materials and manufacturing methods while adhering to the set requirements.

Another discovery during the experiments was that the precise calibration of the mechanism was essential for obtaining the desired stiffness, especially at higher desired output stiffnesses, as the angular difference is much smaller at higher stiffnesses and subsequently requires higher precision. Thus replacing the AS5600 hall effect sensor with an absolute encoder or a large-range potentiometer could lead to better results as the calibration would only need to be done once. A further set of additional sensors could be useful in providing feedback on the configuration and state of the mechanism such as the displacement of the mechanism and a sensor to detect if the mechanism safety is engaged. The first could be done using a sliding potentiometer on the center guide and the latter could be effectively solved by integrating an endstop at the end of the arms. A final concept would be to add strain gauges to the arms, which combined with the angle of the arm, can be transformed to an output force and displacement of the mechanism.

Selecting lighter-weight components that better fit the requirements starting with the motors used would also be required for the next iteration of the mechanism. The motor used to set the stiffness is overpowered for the desired application and the motor in the retraction mechanism is sub-optimal. Additionally, the retraction mechanism should use a non-backlash system as used in the stiffness mechanism to reduce continued power consumption, allowing for better portability of the design. A further refinement would be the addition of a thrust bearing in the stiffness mechanism to better counteract the force from the worm wheel, important for the long-term durability of the mechanism.

Lastly, integrating the mechanism into the exosuit highlighted limitations in both the exosuit design and the mechanism itself, such as a higher than desired friction in both systems, causing the mechanism to underperform. After addressing this and implementing some if not all of the previously mentioned improvements, a follow-up user study can be performed to test the theorized improved performance of a passive-adaptive variable stiffness exosuit.

Acknowledgment

My gratitude goes out to all that have supported me both in my personal and academic journey. Thank you to Cosimo and Sagar for guiding me during the literature research and thesis. Thanks, Giovanni for providing the opportunity to contribute to research which was very fun and allowed me to experience using equipment usually only accessible during the master thesis. Thank you Maria for inspiring me and showing me the possibilities I had available to me. Thank you Mom and Dad for being amazing parents that taught by example and made me who I am today.

References

[1] “Work Safety: Overexertion and Bodily Reaction - Injury Facts,” Jan. 2023, [Online; accessed 17. Aug. 2023]. [Online]. Available: https://injuryfacts.nsc.org/work/safety-topics/overexertion-and-bodily-reaction

[2] P. Maurice, J. Čamernik, D. Gorjan, B. Schirrmeister, J. Bornmann, L. Tagliapietra, C. Latella, D. Pucci, L. Fritzsche, S. Ivaldi, and J. Babič, "Objective and Subjective Effects of a Passive Exoskeleton on Overhead Work," *IEEE Trans. Neural Syst. Rehabil. Eng.*, vol. 28, no. 1, pp. 152–164, Oct. 2019.

[3] M. Xiloyannis, R. Alicea, A.-M. Georgarakis, F. L. Haufe, P. Wolf, L. Masia, and R. Riener, "Soft robotic suits: State of the art, core technologies, and open challenges," *IEEE Transactions on Robotics*, vol. 38, no. 3, pp. 1343–1362, 2022.

[4] S. Joshi, I. Beck, A. Seth, and C. Della Santina, "Minimalistic soft exosuit for assisting the shoulder via biomechanics-aware optimization," in *2022 IEEE-RAS 21st International Conference on Humanoid Robots (Humanoids)*. IEEE, 2022, pp. 667–673.

[5] R. Alami, A. Albu-Schaeffer, A. Bicchi, R. Bischoff, R. Chatila, A. De Luca, A. De Santis, G. Giralt, J. Guiochet, G. Hirzinger, F. Ingrand, V. Lippiello, R. Mattone, D. Powell, S. Sen, B. Siciliano, G. Tonietti, and L. Villani, "Safe and dependable physical human-robot interaction in anthropic domains: State of the art and challenges," in *2006 IEEE/RSJ International Conference on Intelligent Robots and Systems*, 2006, pp. 1–16.

[6] D. Lawrence, "Impedance control stability properties in common implementations," in *Proceedings. 1988 IEEE International Conference on Robotics and Automation*, 1988, pp. 1185–1190 vol.2.

[7] F. J. Abu-Dakka and M. Saveriano, "Variable Impedance Control and Learning—A Review," *Front. Rob. AI*, vol. 7, p. 590681, Dec. 2020.

[8] G. Pratt and M. Williamson, "Series elastic actuators," in *Proceedings 1995 IEEE/RSJ International Conference on Intelligent Robots and Systems. Human Robot Interaction and Cooperative Robots*, vol. 1, 1995, pp. 399–406 vol.1.

[9] T. G. Sugar, "A novel selective compliant actuator," *Mechatronics*, vol. 12, no. 9-10, pp. 1157–1171, 2002.

[10] R. Van Ham, B. Vanderborght, M. Van Damme, B. Verrelst, and D. Lefeber, "Maccepa, the mechanically adjustable compliance and controllable equilibrium position actuator: Design and implementation in a biped robot," *Robotics and Autonomous Systems*, vol. 55, no. 10, pp. 761–768, 2007.

[11] S. Wolf and G. Hirzinger, "A new variable stiffness design: Matching requirements of the next robot generation," in *2008 IEEE International Conference on Robotics and Automation*. IEEE, 2008, pp. 1741–1746.

[12] R. v. Ham, T. Sugar, B. Vanderborght, K. Hollander, and D. Lefeber, "Compliant actuator designs," *IEEE Robotics & Automation Magazine*, vol. 3, no. 16, pp. 81–94, 2009.

[13] B. Vanderborght, N. G. Tsagarakis, R. Van Ham, I. Thorson, and D. G. Caldwell, "Maccepa 2.0: compliant actuator used for energy efficient hopping robot chobino1d," *Autonomous Robots*, vol. 31, pp. 55–65, 2011.

[14] S. Wolf, O. Eiberger, and G. Hirzinger, "The dlr fsj: Energy based design of a variable stiffness joint," in *2011 IEEE international conference on robotics and automation*. IEEE, 2011, pp. 5082–5089.

[15] G. Tonietti, R. Schiavi, and A. Bicchi, "Design and control of a variable stiffness actuator for safe and fast physical human/robot interaction," in *Proceedings of the 2005 IEEE international conference on robotics and automation*. IEEE, 2005, pp. 526–531.

[16] S. A. Migliore, E. A. Brown, and S. P. DeWeerth, "Biologically inspired joint stiffness control," in *Proceedings of the 2005 IEEE international conference on robotics and automation*. IEEE, 2005, pp. 4508–4513.

[17] J. W. Hurst, J. E. Chestnutt, and A. A. Rizzi, "The actuator with mechanically adjustable series compliance," *IEEE Transactions on Robotics*, vol. 26, no. 4, pp. 597–606, 2010.

[18] T. Morita and S. Sugano, "Design and development of a new robot joint using a mechanical impedance adjuster," in *Proceedings of 1995 IEEE International Conference on Robotics and Automation*, vol. 3. IEEE, 1995, pp. 2469–2475.

[19] A. Jafari, N. G. Tsagarakis, B. Vanderborght, and D. G. Caldwell, "A novel actuator with adjustable stiffness (awas)," in *2010 IEEE/RSJ International Conference on Intelligent Robots and Systems*. IEEE, 2010, pp. 4201–4206.

[20] A. Jafari, N. G. Tsagarakis, and D. G. Caldwell, "Awas-ii: A new actuator with adjustable stiffness based on the novel principle of adaptable pivot point and variable lever ratio," in *2011 IEEE International Conference on Robotics and Automation*. IEEE, 2011, pp. 4638–4643.

[21] S. S. Groothuis, G. Rusticelli, A. Zucchelli, S. Stramigioli, and R. Carloni, "The vsaut-ii: A novel rotational variable stiffness actuator," in *2012 IEEE International Conference on Robotics and Automation*. IEEE, 2012, pp. 3355–3360.

[22] ——, "The variable stiffness actuator vsaut-ii: Mechanical design, modeling, and identification," *IEEE/ASME Transactions on Mechatronics*, vol. 19, no. 2, pp. 589–597, 2014.

[23] M. K. Shepherd and E. J. Rouse, "The vspa foot: A quasi-passive ankle-foot prosthesis with continuously variable stiffness," *IEEE Transactions on Neural Systems and Rehabilitation Engineering*, vol. 25, no. 12, pp. 2375–2386, 2017.

[24] S. Mghames, M. Laghi, C. Della Santina, M. Garabini, M. Catalano, G. Grioli, and A. Bicchi, "Design, control and validation of the variable stiffness exoskeleton flexo," in *2017 International Conference on Rehabilitation Robotics (ICORR)*, 2017, pp. 539–546.

[25] S. O. Schrade, K. Dätwyler, M. Stücheli, K. Studer, D.-A. Türk, M. Meboldt, R. Gassert, and O. Lambercy, "Development of varileg, an exoskeleton with variable stiffness actuation: first results and user evaluation from the cybathlon 2016," *Journal of neuroengineering and rehabilitation*, vol. 15, pp. 1–18, 2018.

[26] Y. Liu, S. Guo, H. Hirata, H. Ishihara, and T. Tamiya, "Development of a powered variable-stiffness exoskeleton device for elbow rehabilitation," *Biomed. Microdevices*, vol. 20, no. 3, pp. 1–13, Sep. 2018.

[27] C. M. Thalman, J. Hsu, L. Snyder, and P. Polygerinos, "Design of a soft ankle-foot orthosis exosuit for foot drop assistance," in *2019 International Conference on Robotics and Automation (ICRA)*. IEEE, 2019, pp. 8436–8442.

[28] W. He, W. Zhang, and X. Ding, "Self adjusting exosuit for shoulder," in *Intelligent Robotics and Applications: 14th International Conference, ICIRA 2021, Yantai, China, October 22–25, 2021, Proceedings, Part I 14*. Springer, 2021, pp. 717–727.

[29] S. K. Au, H. Herr, J. Weber, and E. C. Martinez-Villalpando, "Powered ankle-foot prosthesis for the improvement of amputee ambulation," in *2007 29th annual international conference of the IEEE engineering in medicine and biology society*. IEEE, 2007, pp. 3020–3026.

[30] "Trinamic," Jul. 2023, [Online; accessed 15. Jul. 2023]. [Online]. Available: https://www.trinamic.com/products/drives/bldc-motors-details/qbl4208

[31] "Framo Morat Shop | Center distance 31," Jul. 2023, [Online; accessed 15. Jul. 2023]. [Online]. Available: https://shop.framo-morat.com/en/Worm-gear-sets/Center-distance-31/?force_sid=jp2t3ogsm41a0fomhjd9kqu1v7

[32] "AS5600 - ams," Jul. 2023, [Online; accessed 15. Jul. 2023]. [Online]. Available: https://ams.com/en/as5600

[33] Y. Name, "ROBOTIS e-Manual," Jul. 2023, [Online; accessed 17. Aug. 2023]. [Online]. Available: https://emanual.robotis.com/docs/en/dxl/x/xm430-w210